ISSN 1063-7761, Journal of Experimental and Theoretical Physics, 2020, Vol. 131, No. 4, pp. 558–565. © Pleiades Publishing, Inc., 2020.
Russian Text © The Author(s), 2020, published in Zhurnal Eksperimental'noi i Teoreticheskoi Fiziki, 2020, Vol. 158, No. 4, pp. 636–644.

SOLIDS AND LIQUIDS

Second Harmonic Generation in Arrays of Nanoholes in a Silver Film

I. A. Kolmychek[a,*], E. A. Mamonov[a], A. A. Ezhov[a,b,c], O. Yu. Rogov[b,d], V. V. Artemov[b], M. V. Gorkunov[b], and T. V. Murzina[a]

[a] *Faculty of Physics, Moscow State University, Moscow, 119991 Russia*
[b] *Shubnikov Institute of Crystallography, Federal Scientific Research Center "Crystallography and Photonics," Russian Academy of Sciences, Moscow, 119333 Russia*
[c] *Quantum Technology Center, Moscow State University, Moscow, 119899 Russia*
[d] *Skolkovo Institute of Science and Technology, Moscow, 143025 Russia*
**e-mail: irisha@shg.ru*

Received March 20, 2020; revised April 16, 2020; accepted April 20, 2020

Abstract—Specific features of optical second harmonic (SH) generation in arrays of chiral helical nanoholes in a silver film are studied experimentally. An increase in the intensity of the second-order nonlinear optical response is observed in the region of anomalous resonant transmission. The significant role of the rotational symmetry of the array of nanoholes in the formation of the SH response is revealed, which determines the azimuthal dependence of both the intensity of the second-order optical signal and the SH circular dichroism.

DOI: 10.1134/S1063776120090174

1. INTRODUCTION

Optics of metallic nanostructures has become an important and rapidly developing area of world science in the last decade [1]. This is associated, on the one hand, with significant progress in the manufacturing technologies (explosive, colloidal lithography, etc.) for nanostructures and, on the other hand, with the possible applications of the studied phenomena in functional nanophotonic devices for the control over the parameters of optical radiation, sensorics, and optical switching. As is known, in metal particles of subwavelength size, localized surface plasmons can be excited in the optical range; this fact is used to improve the efficiency of interaction of light with such particles. Optical properties of metal nanoparticles of various shapes (spherical, cylindrical, chiral, "core–shell," etc.) have been studied theoretically and experimentally in [2–7]. A significant disadvantage of these structures is a substantial decrease in light transmission in the spectral region of excitation of a local plasmon, which, in turn, reduces the efficiency of the control over the parameters of optical radiation. A fundamentally different design of the structure is an inverted structure, namely, a lattice of cylindrical nanoholes with the diameter of 150 nm in a 200-nm-thick silver film, which was first proposed by Ebbessen in 1998 [8]. It was found that, upon excitation of surface plasmons at the inner boundary of subwavelength nanoholes, the whole structure exhibits the so-called anomalous light transmission, when the transmittance exceeds the value determined by the total area of the holes in the structure. The mechanism of this effect is that the excited plasmons lead to an increase in the evanescent field near the film surface, and, after this enhanced field tunnels through the holes, the reverse transformation of the surface plasmons into the radiation field occurs [9].

Subsequently, various research groups used various metals [10] and shapes of nanoholes (square [11], H-shaped [12], X-shaped [13], I-shaped [14], etc.) to achieve the most effective field enhancement and to maximize the transmittance. These works were stimulated by possible applications of hole structures in sensorics based on the sensitivity of the resonant properties to the refractive index of the surrounding dielectric medium or on the selective enhancement of Raman scattering [15–18]. In addition, a design of planar chiral nanoholes (in the form of a gammadion) in a metal film was proposed; in this case, different localizations of the electric field in the structure are observed for right and left circular polarizations of the probe radiation, which leads to a change in the polarization state of light transmitted through the structure [19]. Thus, the analysis of the electromagnetic field localization in a structure is important for evaluating the efficiency of the excitation of local plasmons in metallic nanostructured films and their functional properties.

The method of second harmonic (SH) generation is highly sensitive to the resonant properties of nanostructured materials [20]; therefore, it is widely used to

study plasmon structures and metasurfaces, including arrays of nanoholes of various shapes, in which an increase in the SH generation intensity is observed in the range of anomalous transmission [21–23]. For example, in [24], the authors calculated the linear optical spectra of square arrays of triangular nanoholes in a metal film and observed an increase in the second-order nonlinear optical response in the region of excitation of localized and surface plasmon polaritons due to the enhancement of the fundamental field in the near-surface area of the film.

As a rule, the chirality effects manifest themselves much stronger in the nonlinear optical response as compared to the linear one. This was demonstrated for arrays of planar chiral nanoelements of various shapes [25–28]. In addition, in the nonlinear optical response, fundamentally new effects may appear due to the chirality of metasurfaces, that do not have linear-optical analogs; these effects include the asymmetry of the SH generation and the so-called inverse dichroism [29]. It was also shown that, based on the analysis of the parameters of the nonlinear optical response, it is possible to distinguish the type of enantiomers, i.e., the sign of the chirality of a metasurface.

In the case of three-dimensional nanostructures, one can expect a significant enhancement of the second-order nonlinear optical effects due to chirality. Thus, large values of the angle of rotation of the polarization plane of the SH radiation up to 45° were found in metal nanohelices [30, 31]. At the same time, similar experiments have not been carried out on inverted structures. In the present study, we consider the effects of the SH generation in arrays of three-dimensional chiral nanoholes in a silver film of submicron thickness.

2. SAMPLES

The arrays of nanoholes were fabricated by focused ion beam (FIB) etching of gallium Ga+ ions using an FEI Scios DualBeam electron microscope [32]. The structures were formed in a 250-nm-thick silver film deposited by thermal evaporation in vacuum (10^{-5} Pa) onto a 80-nm-thick supporting silicon oxide membrane. The arrays of chiral holes were fabricated at a screen magnification of a scanning electron microscope ×7000, an accelerating voltage of 30 kV, and an ion beam current of 0.1 nA. Complex three-dimensional shape of the nanoholes was provided by the controlled movement of the FIB in accordance with digital templates. All templates were designed as circles with a diameter of 3600 pixels, which provided arrays of holes filling identical circular areas with a diameter of 35 μm. We fabricated and investigated four arrays of chiral holes (see Fig. 1): arrays with rotational symmetry of the third and sixth orders (with point symmetry groups C_3 and C_6, respectively), which consisted of C_3 and C_6 symmetry holes located at the nodes of a triangular lattice; an array with rotational symmetry of the fourth order (with point symmetry group C_4), which consisted of C_4 symmetry holes located at the nodes of a square lattice; and an array of C_5 symmetry holes located at the nodes of the Penrose mosaic, which had (as a whole) rotational symmetry of the fifth order (point group C_5). In what follows, we will denote the arrays by the type of their point symmetry group, respectively, as C_3, C_4, C_5, and C_6. The through parts of all screw-shaped nanoholes have a diameter of about 200 nm. The subwavelength periodicity of the samples C_3, C_4, and C_6 made it possible to exclude the diffraction of visible light. In the quasiperiodic array C_5, the mean distance between the holes is also subwavelength.

3. EXPERIMENTAL SETUPS, MEASUREMENT METHODS, AND RESULTS

3.1. Linear Optical Response

The transmission spectroscopy of the samples was carried out by two independent methods: by a modified confocal laser scanning microscope (CLSM) and by a setup based on a spectroscopic ellipsometer (SE).

When carrying out measurements, we first used an Olympus FluoView FV1000 CLSM, which is based on an Olympus IX81 inverted optical microscope and equipped with a scanning device with a spectral detection system. As a source of transmitted light, we used a Schott ACE I illuminator with a 150 W halogen lamp and radiation output through a fiber optic bundle. To expand the spectral range of the source, we removed the built-in heat-shielding light filter from the light source before measurements.

Alternative studies were carried out on a setup based on a UVISEL 2 Horiba Jobin-Yvon spectroscopic ellipsometer and an Ocean Optics USB4000 fiber-optic spectrometer, which replaced the standard spectrometer included in the ellipsometer, thus significantly reducing the measurement time of the spectra. The light source was a 150 W short-arc xenon lamp. This setup made it possible to measure the transmission spectra of light with a given linear polarization depending on the orientation of the polarization plane of light (the azimuthal angle). In both methods, the light intensity was normalized to the spectrum of a hole of 33.7 μm in diameter that was specially made near the arrays of chiral nanoholes. It should be noted that the features in the transmission spectra obtained by two independent methods coincided with high accuracy.

The transmission spectra of the samples are presented in Fig. 2a and demonstrate regions of anomalously high light transmission in the optical range, the amplitude and the spectral position of the maximum depending significantly on the symmetry of the array. The effect is most pronounced for the sample C_3, for which the transmission increases to 60% in the wave-

length range of 680–690 nm. In the sample C_4, the anomalous transmission is much less pronounced. To study the circular dichroism of the structures, we measured the transmission spectra of light with right and left circular polarizations, which were formed by a Moxtek UBB01A ultrawideband (wire-grid) polarizer in combination with a Thorlabs AQWP05M-600 achromatic quarter-wave plate. Radiation with circular polarizations of opposite signs was obtained by changing the mutual orientation of these elements. The measurements were carried out using a modified CLSM. The magnitude of the circular dichroism of optical radiation transmitted through the samples was calculated by the formula

$$CD = \frac{T^{\text{right}} - T^{\text{left}}}{T^{\text{right}} + T^{\text{left}}},$$

where T^{right} and T^{left} are the transmission coefficients for the right and left circular polarizations of the light incident on the structure. The corresponding results are shown in Fig. 2b; they confirm that the magnitude and sign of the circular dichroism of transmission depend significantly on the symmetry of the nanoholes and their packing in the array. The sample C_5 with the elements located at the nodes of the Penrose mosaic shows almost no circular dichroism in the entire visible wavelength range. Other arrays show an up to 60% increase in circular dichroism.

3.2. Second Harmonic Generation

Nonlinear optical experiments were carried out using a setup based on a tunable pulsed titanium–sapphire laser with a wavelength range of 740–900 nm, a pulse repetition rate of 80 MHz, a pulse duration of 60 fs, and an average power on the sample of 20 mW, which was used as a source of probing radiation. Laser radiation was focused by a lens to a spot with a diameter of about 30 μm on the surface of the structure, thus illuminating more than 10000 nanoholes. A photomultiplier was used to detect the intensity of the SH radiation transmitted through the sample at normal incidence of laser radiation on the structure. The polarization of the probing radiation was set by half-wavelength or quarter-wavelength plates, and the polarization of the nonlinear optical signal was detected by an analyzer (a Glan–Taylor prism).

We carried out experiments to investigate the SH generation for circularly polarized radiation at the fundamental frequency and the detection of the total intensity of the second-order nonlinear optical response. From the data obtained, we calculated the spectra of the SH intensity and the circular dichroism of the SH:

$$I_{2\omega} = (I_{2\omega}^{\text{right}} + I_{2\omega}^{\text{left}})/2,$$

$$SHGCD = \frac{I_{2\omega}^{\text{right}} - I_{2\omega}^{\text{left}}}{I_{2\omega}^{\text{right}} + I_{2\omega}^{\text{left}}},$$

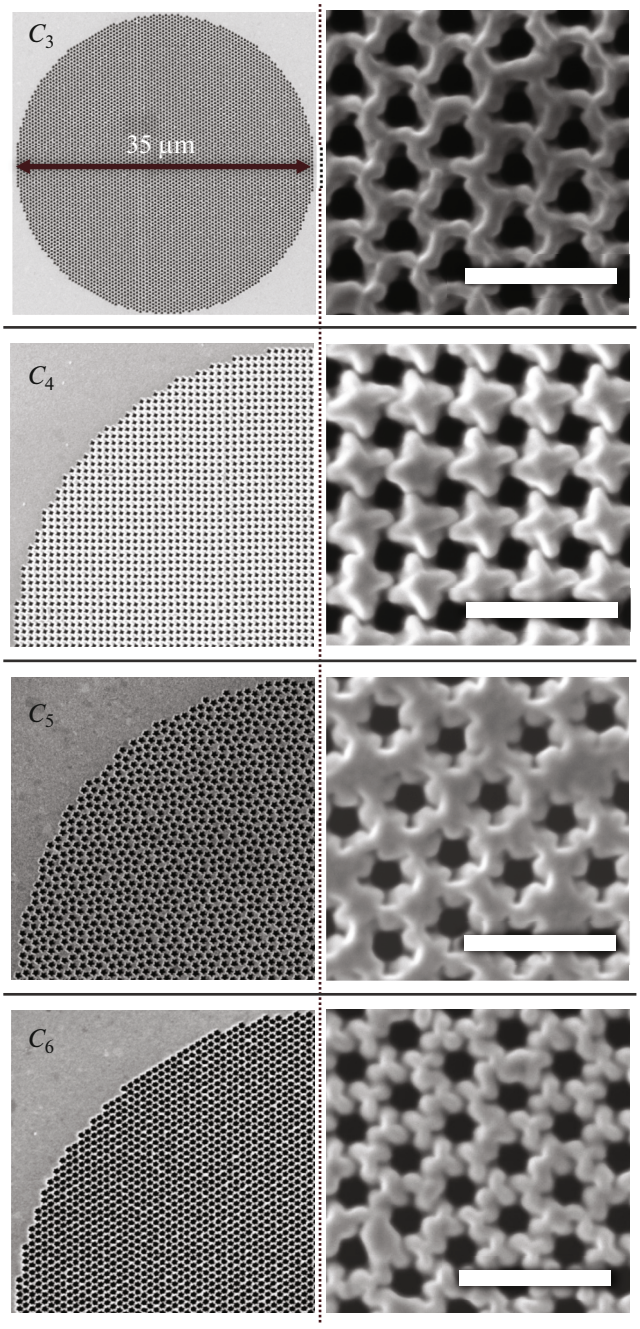

Fig. 1. SEM images of the structures. (left) Full sample C_3 and a quarters of samples C_4, C_5, and C_6. (right) SEM images of fragments of the corresponding samples obtained at higher magnification with 1 μm marks.

where $I_{2\omega}^{\text{right}}$ and $I_{2\omega}^{\text{left}}$ are the SH intensities for the right and left circularly polarized incident radiation. The corresponding results are demonstrated in Fig. 3. One can see that different samples exhibit qualitatively similar SH spectral dependence; a decrease in the SH signal is observed when the wavelength of the probe radiation is shifted to the long-wavelength region. The most effective SH generation occurs in the sample C_3.

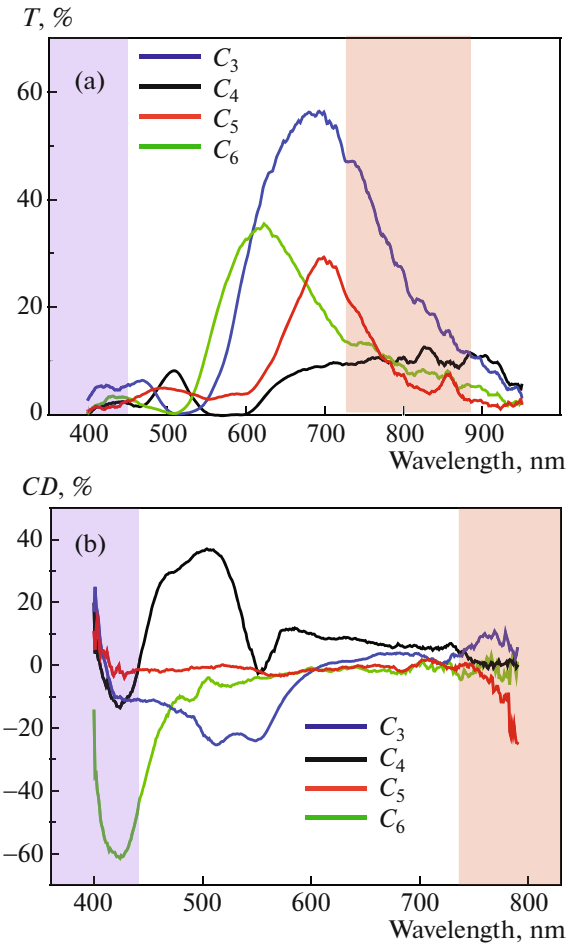

Fig. 2. Linear optical properties of the arrays of nanoholes: (a) transmission spectra and (b) circular dichroism spectra. The spectral regions of tuning of the Ti:Sa laser and the generated SH are highlighted in pink and blue.

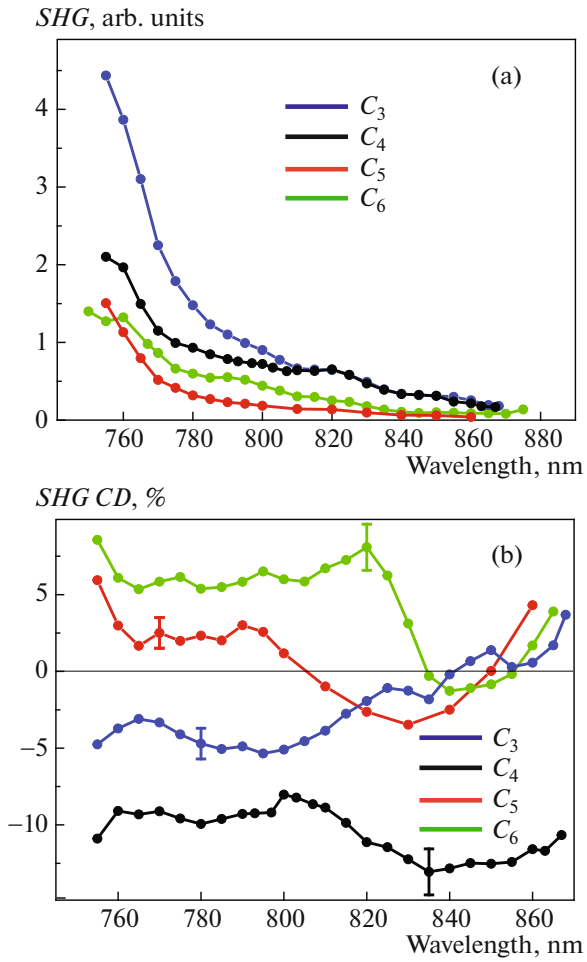

Fig. 3. (a) SH intensity spectra from arrays of holes of different symmetry for circularly polarized probe radiation. (b) Spectra of circular dichroism of the second harmonic generation.

As follows from Fig. 3b, the sign and magnitude of the circular dichroism of the SH field substantially depend on the symmetry of the sample. Maximum dichroism of about 10–12% is observed in the sample C_4. In the considered spectral range, the circular dichroism of the structures C_3, C_5, and C_6 passes through zero once or twice and, accordingly, changes its sign.

The measurements of the azimuthal anisotropy of the SH intensity upon irradiation of the structure with linearly polarized light were carried out for a fixed sample for a synchronous rotation of the polarization plane of the probe radiation (rotation of the $\lambda/2$ plate through an angle $\theta/2$) and the SH radiation (rotation of the analyzer through an angle θ). The experiments were carried out on the samples C_3 and C_4 for two combinations of polarizations of the laser and SH radiation: when the polarization planes of the incident and detected radiation were parallel and perpendicular to each other.

As follows from the experimental results, in the case of linear polarization of the laser radiation, the SH signal from both samples is anisotropic. The SH intensity spectra for different azimuthal orientations of the polarization plane of the incident radiation in sample C_3 are shown in Fig. 4. For both parallel and perpendicular orientations of the polarizations of the fundamental and the SH radiation, the azimuthal dependence of the SH radiation has six maxima; the angular position of the maxima in the first case (Fig. 4a) coincides with the position of the minima in the second case (Fig. 4b). This is more clearly seen in the left panels, where the experimental azimuthal dependence of the SH intensity in polar coordinates is superimposed with the position of the sample. It should be noted that the SH intensity averaged over the azimuthal position of the sample increases with decreasing laser wavelength in accordance with the data in Fig. 3a.

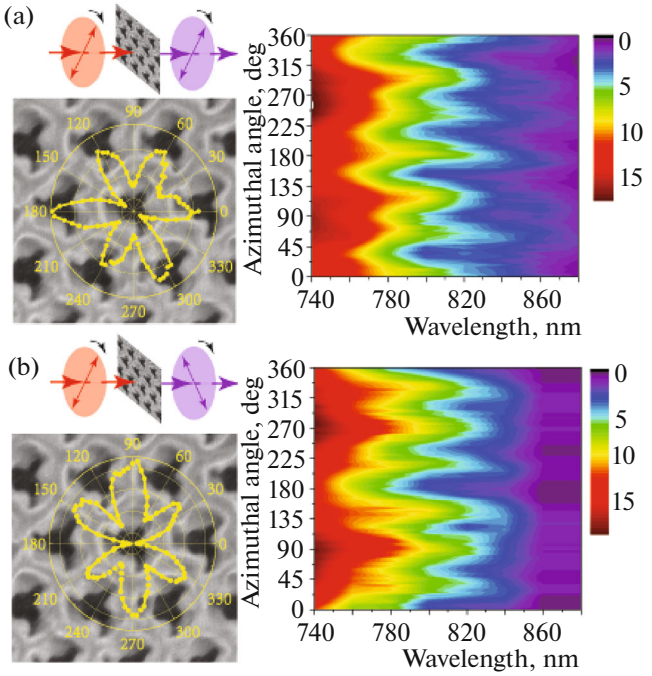

Fig. 4. SH generation intensity spectra for different azimuthal positions of the C_3 sample for parallel (a) and orthogonal (b) linear polarizations of the probe and SH radiation. In the right panels, the color indicates the SH intensity. The left panels demonstrate the experimental schemes and the orientations of the azimuthal positions of the SH maxima relative to the structure at a laser wavelength of 820 nm.

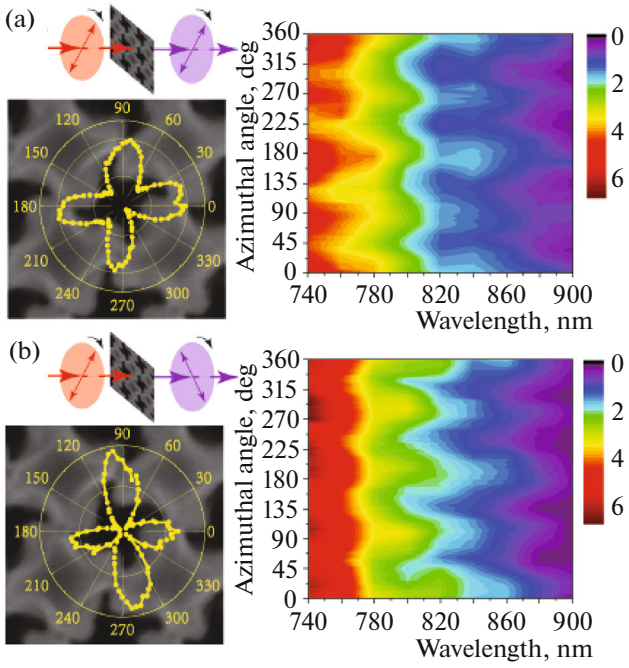

Fig. 5. SH generation intensity spectra for different azimuthal positions of the C_4 sample for parallel (a) and orthogonal (b) polarizations of the probe and SH radiation. In the right panels, the color indicates the SH intensity. The left panels demonstrate the experimental schemes and the orientations of the azimuthal positions of the SH maxima relative to the structure at a laser wavelength of 800 nm.

The results of the anisotropy of the SH intensity in the sample C_4 are shown in Fig. 5. For both parallel and perpendicular orientations of the polarizations of the incident and detected radiation, the azimuthal dependence of the SH has four maxima, but the angular position of the maxima in the first case (Fig. 5a) is shifted clockwise relative to the edge of the holes' lattice by approximately 5°–10°, while, in the second case, it is shifted in the opposite direction (Fig. 5b). This also follows from the graphs shown in the left panels, where the experimental azimuthal dependence of the SH intensity in polar coordinates is superimposed on the sample position. It should also be noted that, in this case, the SH intensity averaged over the azimuthal position of the sample increases with decreasing wavelength of the probe radiation, just as in the case of circularly polarized fundamental radiation.

4. DISCUSSION

First of all, note that, in the samples under study, the distances between the nanoholes are comparable to their lateral dimensions, and the observed optical properties are due to collective effects in the arrays of holes upon irradiation with light. For metallic nanostructures, of key importance are the plasmon resonances that are localized directly near the metal surface and significantly depend on its profile. This explains the qualitative difference between the linear and nonlinear optical properties of the arrays of holes of similar shape in an identical silver film but with different orders of rotational symmetry.

It is known that plasmons are responsible for anomalously high light transmission through arrays of nanoslits and nanoholes [8, 9]. A characteristic feature of the anomalous transmission is the presence of a weak background and a strong resonance contribution, whose interference gives the transmission spectra an asymmetric shape of the Fano-type resonance type [33]; therefore, the spectral positions of the absorption and transmission maxima are slightly shifted both relative to each other and relative to the plasmon resonance wavelength, as was shown earlier in similar structures [34]. It follows from the data shown in Fig. 2a that both the position of the anomalous transmission band and its maximum essentially depend on the shape of the holes and the symmetry of their arrays.

Apparently, the chirality of the linear optical response of screw-shaped metal holes is also of plasmonic nature [34, 35]: these holes exhibit a decrease in the magnitude of the circular dichroism in the plas-

mon resonance region (600–800 nm) under the conditions of anomalously high transmission, which is associated with an increase in the denominator in the corresponding formula. At the same time, at the short-wavelength edge of the anomalous transmission region, the enhancement of circular dichroism is observed, which is due to the noticeable difference in the absorption of left and right circularly polarized radiation (in all structures except for the quasiperiodic array C_5). It is also interesting that the sign of the circular dichroism depends on the symmetry of the array, while, in two-dimensional chiral structures, this sign is determined by the handedness of the chiral structure and is opposite for enantiomers [36].

The nonlinear optical response is significantly enhanced by plasmon resonances, as well as by many other resonances of different nature [1]. For most condensed media, the resonant enhancement of the bulk nonlinearity is adequately described by simple Miller's empirical rule, which implies the proportionality of the nonlinear susceptibility to the product of linear susceptibilities at the frequencies of all interacting waves [37]. Although the high localization of the nonlinear optical response of metallic nanostructures immediately near their surface leads to noticeable quantitative deviations from such a simple proportionality [38], the excitation of plasmons significantly increases the field amplitudes near the surface, which appreciably enhances the SH generation [20, 24]. Such enhancement also takes place in the considered case of arrays of subwavelength holes in a metal film: one can see that the SH intensity increases by more than an order of magnitude as the laser radiation wavelength approaches the plasmon resonances at wavelengths of 600–700 nm (Fig. 3a).

The analysis of the SH intensity spectra for different structures (Fig. 3a) implies that C_3 array exhibits several times higher SH generation efficiency than the others arrays. A simple explanation of this effect is that, in the case of normal incidence of the fundamental plane wave on infinite arrays of scatterers, only the C_3 structure (point symmetry group C_3) can generate SH in the electric dipole approximation [39], i.e., it has nonzero components of the second-order nonlinear susceptibility, while the arrays of other symmetries have no such components.

Indeed, in the absence of the normal component of the electric field, the SH generation in the direction perpendicular to the surface originates from the components of the second-order susceptibility tensor $\chi^{(2)}_{ijk}$ with indices x and y of the coordinate axes in the plane of the structure. The analysis of the symmetry of the second-order nonlinear optical response of an array of nanostructures shows that such components are present only in planar structures with third-order rotational symmetry (the point group C_3) and are determined by the following susceptibility components: $\chi^{(2)}_{xxx} = -\chi^{(2)}_{xyy} = -\chi^{(2)}_{yxy} = -\chi^{(2)}_{yyx}$ and $\chi^{(2)}_{yyy} = -\chi^{(2)}_{yxx} = -\chi^{(2)}_{xxy} = -\chi^{(2)}_{xyx}$ [40]. For parallel linear polarizations of the fundamental and SH waves, the dependence of the SH intensity on the angle ψ between the electric field of the incident wave and the x axis in the plane has the form

$$I_{2\omega}(\psi) \propto |\chi^{(2)}_{xxx}\cos 3\psi - \chi^{(2)}_{yyy}\sin 3\psi|^2.$$

For crossed polarizations of the incident and SH waves, a similar dependence is described by the expression

$$I_{2\omega}(\psi) \propto |\chi^{(2)}_{xxx}\sin 3\psi + \chi^{(2)}_{yyy}\sin 3\psi|^2.$$

The experimental data shown in Fig. 4 fully correspond to these dependences, and the fact that the azimuthal dependences of the SH intensity in Fig. 4 approximately coincide in amplitude and are rotated through 30° relative to each other indicates the equality of the components, $\chi^{(2)}_{xxx} = \chi^{(2)}_{yyy}$. A small isotropic background corresponds to incoherent SH scattering (hyper-Rayleigh scattering) by the structure.

In the array of holes C_4 (the point symmetry group C_4), nonzero components of the second-order susceptibility tensor, which do not have the z index, are absent in the electric dipole approximation [40]. Nevertheless, the experimental data (Fig. 3a) indicate the presence of a noticeable SH signal, which, according to Fig. 5, is also coherent and reflects the fourth-order rotational symmetry. In this case, different mechanisms of SH generation are possible. First, both the spatial inhomogeneity of the laser beam and the presence of structures inclined to the plane of the sample surface ("thread" in screw-shaped holes) can lead to locally nonzero values of the z component of the pump field; in this case, the electric dipole components of the second-order susceptibility tensor will contribute to the nonlinear optical response [40]:

$$\chi^{(2)}_{xxz} = \chi^{(2)}_{xzx} = \chi^{(2)}_{yyz} = \chi^{(2)}_{yzy}, \quad \chi^{(2)}_{zxx} = \chi^{(2)}_{zyy},$$
$$\chi^{(2)}_{xyz} = \chi^{(2)}_{xzy} = -\chi^{(2)}_{yzx} = -\chi^{(2)}_{yzx}, \chi^{(2)}_{zzz}.$$

Second, an electric quadrupole term can contribute to the SH generation, which is attributed to the nonlinear polarization of the form [41, 42]

$$P^Q_i = \chi^{(2)Q}_{ijkl}E_i\nabla_k E_l + \nabla_k\chi^{(2)Q}_{ijkl}E_iE_l,$$

induced in the structure, and the fourth-rank tensor $\chi^{(2)Q}_{ijkl}$ in the case of the fourth-order symmetry has sufficiently many nonzero components:

$$\chi^{(2)Q}_{xxxx}, \chi^{(2)Q}_{xxxy}, \chi^{(2)Q}_{xxyy}, \chi^{(2)Q}_{xyxx}, \chi^{(2)Q}_{xyxy}, \chi^{(2)Q}_{xyyy},$$
$$\chi^{(2)Q}_{yxxx}, \chi^{(2)Q}_{yyyy}, \chi^{(2)Q}_{yyyx}, \chi^{(2)Q}_{yyxx}, \chi^{(2)Q}_{yxyy}, \chi^{(2)Q}_{yxxy}.$$

Both of these mechanisms require the inhomogeneity of the laser radiation field in the plane of the

structure [41], which undoubtedly takes place in a real experiment, where inhomogeneity of the intensity of the probe radiation within the focal spot is inevitable. The small size of the arrays of holes also makes the contribution of the edge regions, to which simple symmetry relationships do not apply, significant.

Chirality of the nonlinear optical properties of arrays of holes of different symmetry is quantitatively expressed in the circular SH dichroism, whose spectra are shown in Fig. 3b. The lowest nonlinear optical chirality is characteristic of the quasiperiodic C_5 array, which also exhibits the weakest linear optical chirality (see Fig. 2b). Presumably, this is due to the lowest surface density of chiral nanoholes in the sample C_5. The C_4 array is clearly distinguished by the doubled values of the SH circular dichroism and by the fact that it retains this level of dichroism in the long-wavelength region of the tuning range of the laser.

5. CONCLUSIONS

We have experimentally studied the specific features of the optical and second-order nonlinear optical response in various arrays of three-dimensional chiral nanoholes in a silver membrane of subwavelength thickness. We have found a strong SH anisotropy, which significantly depends on the symmetry of the structure. The sign and magnitude of the circular dichroism in both the linear and nonlinear optical response is determined by the rotational symmetry of an array and, at the SH frequency, reaches approximately 13% in the sample with a fourth-order symmetry axis (the point symmetry group C_4).

FUNDING

The work of V.V.A and M.V.G on the design and fabrication of arrays of chiral holes was supported by the Ministry of Science and Higher Education of the Russian Federation within the framework of the State Assignment of the Federal Research Center "Crystallography and Photonics" of the Russian Academy of Sciences. The studies were carried out with the use of the equipment of the Center for Collective Use of the Federal Research Center "Crystallography and Photonics" with the support of the Ministry of Science and Higher Education of the Russian Federation, project no. RFMEFI62119X0035. Nonlinear optical studies and their analysis were performed by I.A.K. and E.A.M. with the support of the grant of the President of the Russian Federation MK-5704.2018.2.

REFERENCES

1. V. V. Klimov, *Nanoplasmonics* (Fizmatlit, Moscow, 2009; Pan Stanford, Singapore, 2011).
2. V. Amendola, R. Pilot, M. Frasconi, O. M. Maragò, and M. A. Iatì, J. Phys.: Condens. Matter **29**, 203002 (2017).
3. A. V. Baryshev, H. Uchida, and M. Inoue, J. Opt. Soc. Am. B **30**, 2371 (2013).
4. V. K. Valev, N. Smisdom, A. V. Silhanek, B. De Clercq, W. Gillijns, M. Ameloot, V. V. Moshchalkov, and T. Verbiest, Nano Lett. **9**, 3945 (2009).
5. A. Papakostas, A. Potts, D. M. Bagnall, S. L. Prosvirnin, H. J. Coles, and N. I. Zheludev, Phys. Rev. Lett. **90**, 107404 (2003).
6. S. Linden, A. Christ, J. Kuhl, and H. Giessen, Appl. Phys. B **73**, 311 (2011).
7. T. V. Murzina, I. A. Kolmychek, J. Wouters, Th. Verbiest, and O. A. Aktsipetrov, J. Opt. Soc. Am. B **29**, 138 (2012).
8. T. W. Ebbesen, H. J. Lezec, H. F. Ghaemi, T. Thio, and P. A. Wolff, Nature (London, U.K.) **391**, 667 (1998).
9. T. Thio, K. Pellerin, H. Lezec, R. Linke, and T. Ebbesen, Opt. Phot. News **12** (2001).
10. M. Schwind, B. Kasemo, and I. Zoric, Nano Lett. **13**, 1743 (2013).
11. J. A. H. van Nieuwstadt, M. Sandtke, R. H. Harmsen, F. B. Segerink, J. C. Prangsma, S. Enoch, and L. Kuipers, Phys. Rev. Lett. **97**, 146102 (2006).
12. Z. M. Liu, H. J. Li, H. Q. Xu, and G. T. Cao, Opt. Commun. **285**, 3781 (2012).
13. D. Q. Wang, X. L. Yu, and Q. M. Yu, Nanotechnology **23**, 405201 (2012).
14. Y. Hu, G. Liu, Z. Liu, X. Liu, X. Zhang, Z. Cai, M. Liu, H. Gao, and G. Gu, Plasmonics **10**, 483 (2014).
15. Z. Chen, P. Li, S. Zhang, Y. Chen, P. Liu, and H. Duan, Nanotechnology **30**, 335201 (2019).
16. S. Larson, D. Carlson, B. Ai, and Y. Zhao, Phys. Chem. Chem. Phys. **21**, 3771 (2019).
17. D. Jones, N. Liu, B. Corbett, P. Lovera, A. J. Quinn, and A. O'Riordan, J. Phys.: Conf. Ser. **307**, 012005 (2011).
18. P. Candeloro, E. Iuele, G. Perozziello, M. L. Coluccio, F. Gentile, N. Malara, V. Mollace, and E. Fabrizio, Microelectron. Eng. **175**, 30 (2017).
19. A. V. Krasavin, A. S. Schwanecke, N. I. Zheludev, M. Reichelt, T. Stroucken, S. W. Koch, and E. M. Wright, Appl. Phys. Lett. **86**, 201105 (2005).
20. A. Wokaun, J. G. Bergman, J. P. Heritage, A. M. Glass, P. F. Liao, and D. H. Olson, Phys. Rev. B **24**, 849 (1981).
21. B.-L. Wang, R. Wang, R. J. Liu, X. H. Lu, J. Zhao, and Z.-Y. Li, Sci. Rep. **3**, 2358 (2013).
22. H. Lu, X. Liu, R. Zhou, Y. Gong, and D. Mao, Appl. Opt. **49**, 2347 (2010).
23. R. Zhou, H. Lu, X. Liu, Y. Gong, and D. Mao, J. Opt. Soc. Am. B **27**, 2405 (2010).
24. E. Drobnyh and M. Sukharev, J. Chem. Phys. **152**, 094706 (2020).
25. B. K. Canfield, S. Kujala, K. Laiho, K. Jefimovs, J. Turunen, and M. Kauranen, Opt. Express **14**, 950 (2006).
26. S. Chen, F. Zeuner, M. Weismann, B. Reineke, G. Li, V. K. Valev, K. W. Cheah, N. C. Panoiu, Th. Zentgraf, and S. Zhang, Adv. Mater. **28**, 2992 (2016).

27. E. A. Mamonov, T. V. Murzina, I. A. Kolmychek, A. I. Maydykovsky, V. K. Valev, A. V. Silhanek, T. Verbiest, V. V. Moshchalkov, and O. A. Aktsipetrov, Opt. Express **20**, 8518 (2012).
28. E. A. Mamonov, I. A. Kolmychek, S. Vandendriessche, M. Hojeij, Y. Ekinci, V. K. Valev, T. Verbiest, and T. V. Murzina, Phys. Rev. B **89**, 121113(R) (2014).
29. V. K. Valev, A. V. Silhanek, N. Verellen, W. Gillijns, P. van Dorpe, O. A. Aktsipetrov, G. A. E. Vandenbosch, V. V. Moshchalkov, and T. Verbiest, Phys. Rev. Lett. **104**, 127401 (2010).
30. J. T. Collins, D. C. Hooper, A. G. Mark, Ch. Kuppe, and V. K. Valev, ACS Nano **12**, 5445 (2018).
31. D. C. Hooper, A. G. Mark, Ch. Kuppe, J. T. Collins, P. Fischer, and V. K. Valev, Adv. Mater. **29**, 1605110 (2017).
32. O. Yu. Rogov, V. V. Artemov, M. V. Gorkunov, A. A. Ezhov, and S. P. Palto, in *Proceedings of the 15th IEEE International Conference on Nanotechnology, 2015,* p. 136.
33. C. Genet, M. P. van Exter, and J. P. Woerdman, Opt. Commun. **225**, 331 (2003).
34. A. V. Kondratov, M. V. Gorkunov, A. N. Darinskii, R. V. Gainutdinov, O. Y. Rogov, A. A. Ezhov, and V. V. Artemov, Phys. Rev. B **93**, 195418 (2016).
35. M. V. Gorkunov, A. A. Ezhov, V. V. Artemov, O. Y. Rogov, and S. G. Yudin, Appl. Phys. Lett. **104**, 221102 (2014).
36. M. Kuwata-Gonokami, N. Saito, Y. Ino, M. Kauranen, K. Jefimovs, T. Vallius, J. Turunen, and Y. Svirko, Phys. Rev. Lett. **95**, 227401 (2005).
37. R. C. Miller, Appl. Phys. Lett. **5**, 17 (1964).
38. K. O'Brien, H. Suchowski, J. Rho, A. Salandrino, B. Kante, X. Yin, and X. Zhang, Nat. Mater. **14**, 379 (2015).
39. K. Konishi, T. Higuchi, J. Li, J. Larsson, S. Ishii, and M. Kuwata-Gonokami, Phys. Rev. Lett. **112**, 135502 (2014).
40. P. Guyot-Sionnest, W. Chen, and Y. R. Shen, Phys. Rev. B **33**, 8254 (1986).
41. M. Kauranen, T. Verbiest, and A. Persoons, J. Mod. Opt. **45**, 403 (1998).
42. O. A. Aktsipetrov, I. M. Baranova, and K. N. Evtyukhov, *Second Order Nonlinear Optics of Silicon and Silicon Nanostructures* (Fizmatlit, Moscow, 2012; CRC, Boca Raton, FL, 2020).

Translated by I. Nikitin